Contact Analysis of Gears Using a Combined Finite Element and Surface Integral Method

S. M. Vijayakar
Advanced Numerical Solutions, Columbus, OH

Donald R. Houser,
Ohio State University, Columbus, OH

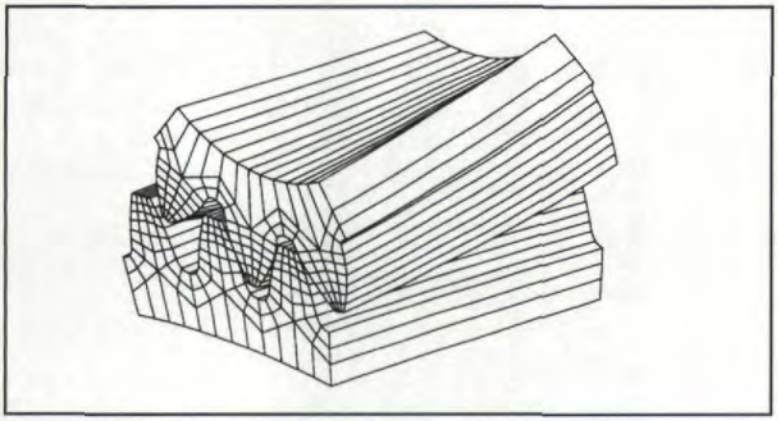

Fig. 1 — Contact analysis of helical gears.

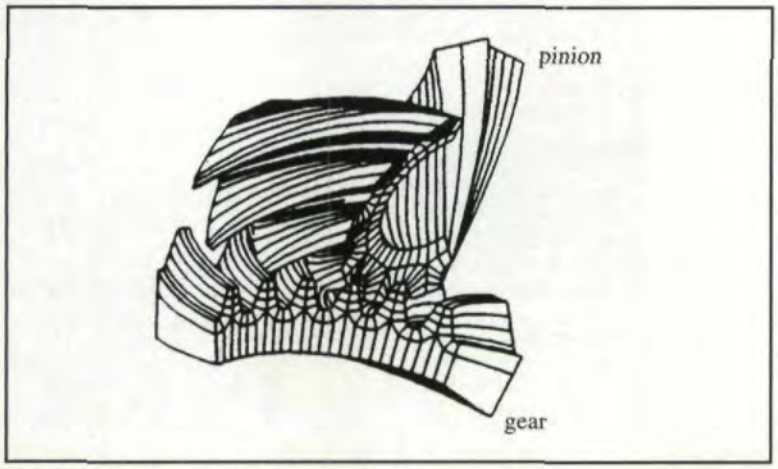

Fig. 2 — Contact analysis of hypoid gears.

Introduction

The complete and accurate solution to the contact problem of three-dimensional gears has been, for the past several decades, one of the more sought after, albeit elusive goals in the engineering community. Even the arrival on the scene in the mid-seventies of finite element techniques failed to produce the solution to any but the most simple gear contact problems.

The reasons for this are manifold. When gears are brought into contact, the width of the contact zone is typically an order of magnitude smaller than the other dimensions of the gears. This gives rise to the need for a very highly refined finite element mesh near the contact zone. But given the fact that the contact zone moves over the surface of the gear, one would need a very highly refined mesh all over the contacting surface. Finite element models refined to this extent cannot be accommodated on even the largest of today's computers. Compounding this difficulty is the fact that the contact conditions are very sensitive to the geometry of the contacting surfaces. General purpose finite element models cannot provide the required level of geometric accuracy. Finally, the difficulties of generating an

optimal three-dimensional mesh that can accurately model the stress gradients in the critical regions, while minimizing the number of degrees of freedom of the model have kept the finite element method from being widely used to solve the complete gear contact problem.

Research in the mid- and late eighties showed that the gear contact problem was not unsurmountable, but required an approach that combined the strengths of the finite element method with those of other techniques, such as the boundary element and surface integral methods. Concepts from mathematical programming could be used to advantage in solving the contact equations. An innovative approach to the formulation of the finite elements themselves could go a long way towards solving the mesh generation and geometric accuracy problems. With the idea of incorporating the best of these and other technologies in mind, we began development of what is now CAPP (Contact Analysis Program Package) four years ago. It has evolved into a powerful collection of computer programs that provide the gear designer with an insight into the state of stress in gears that has thus far never been possible. Some of the features that CAPP supports are friction, sub-surface stress calculation, stress contours, transmission error, contact pressure distributions, and load distribution calculation.

Figs. 1-5 show examples of gear sets for which this process has been successfully used.

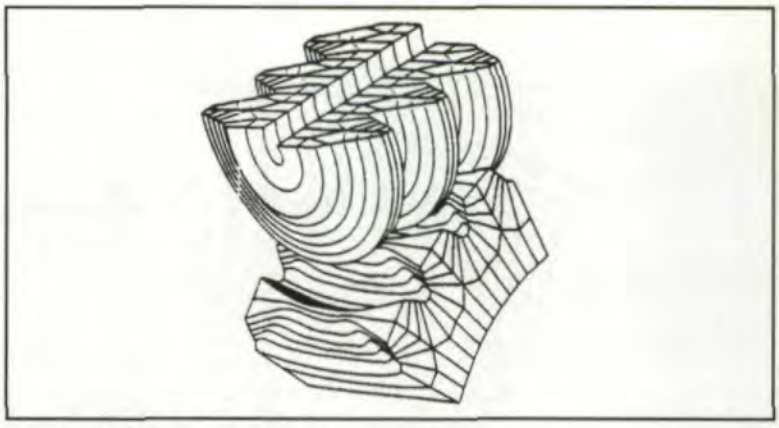

Fig. 3 — Contact analysis of worm gears.

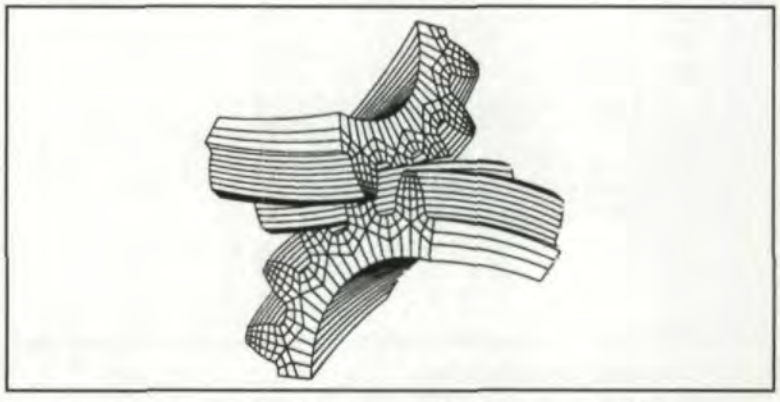

Fig. 4 — Contact analysis of a 90° crossed axis external helical gear set.

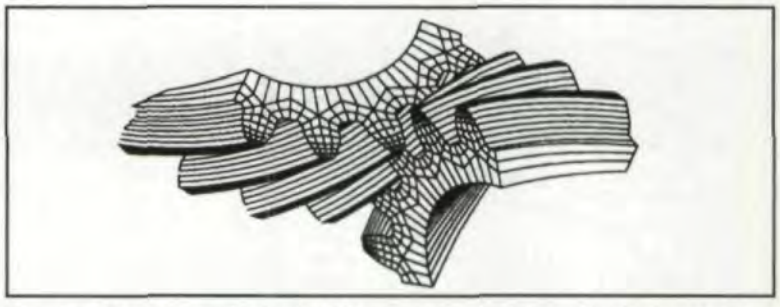

Fig. 5 — Contact analysis of a 90° crossed axis external helical gear set.

Contact Analysis

In earlier studies of contact modeling (See Refs. 1, 2, 11, 12), a pure finite element approach was used to obtain compliance terms relating traction at one location of a body to the normal displacement at another location on the contacting body. It became apparent that in order to obtain sufficient resolution in the contact area, the size of the finite element model would have to be inordinately large. A finite element mesh that is locally refined around the contact region cannot be used when the contact zone travels over the surfaces of the two bodies.

Other researchers working in the tribology area (Refs. 3, 7, 9) have obtained compliance relationships in surface integral form by integrating the Greens function for a point load on the surface of a half space (the Bousinesq solution) over the areas of individual cells demarcated on the contact zone. This method works well as long as the extent of the contacting bodies is much larger than the dimensions of the contact zone, and the contact zone is far enough from the other surface boundaries so that the two contacting bodies may be treated as elastic half spaces. These conditions are, however, not satisfied by gears.

The approach that is described here is based on the assumption that beyond a certain distance from the contact zone, the finite element model predicts deformations well. The elastic half space model is accurate in predicting *relative* displacements of points near the contact zone. Under these assumptions, it is possible to make predictions of surface displacements that make use of the advantages of both the finite element method as well as the surface integral approach.

This method is related to asymptotic matching methods that are commonly used to solve singular perturbation problems. Schwartz and

Dr. S. M. Vijayakar
is the principal at Advanced Numerical Systems, an engineering consulting firm specializing in special purpose finite element and other modeling techniques for the gearing industry.

Dr. D. R. Houser
is Professor of Mechanical Engineering at Ohio State University and the Director of the Gear Dynamics and Gear Noise Research Laboratory at the university.

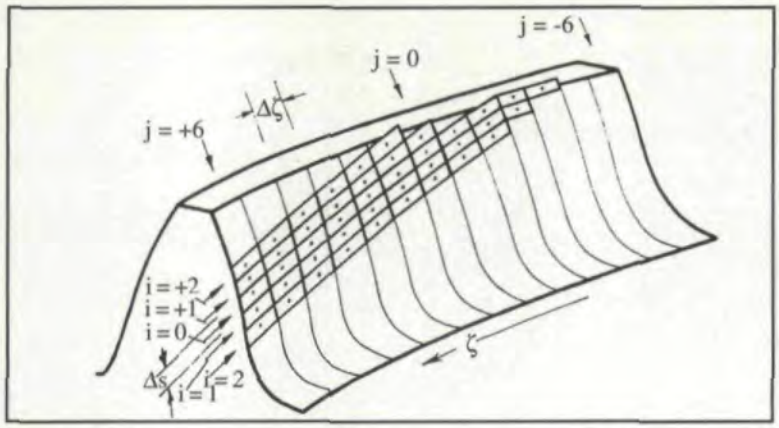

Fig. 6 — Computational grid in the contact zone of the gears.

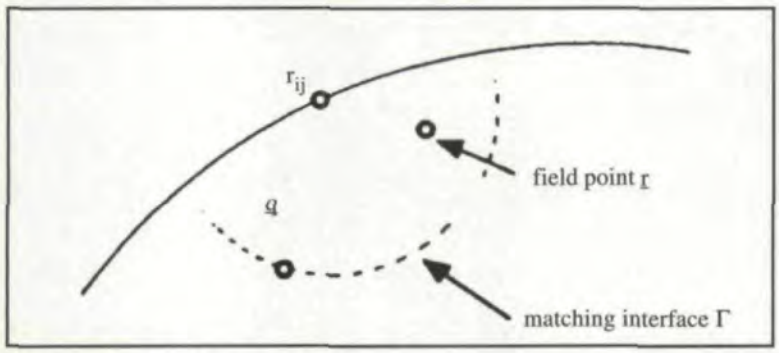

Fig. 7 — The matching interface.

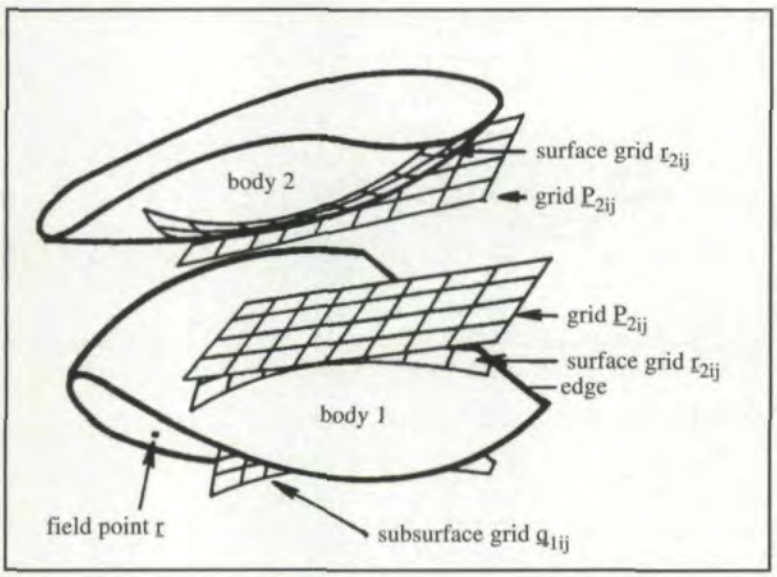

Fig. 8 — The contacting bodies and the computational grids.

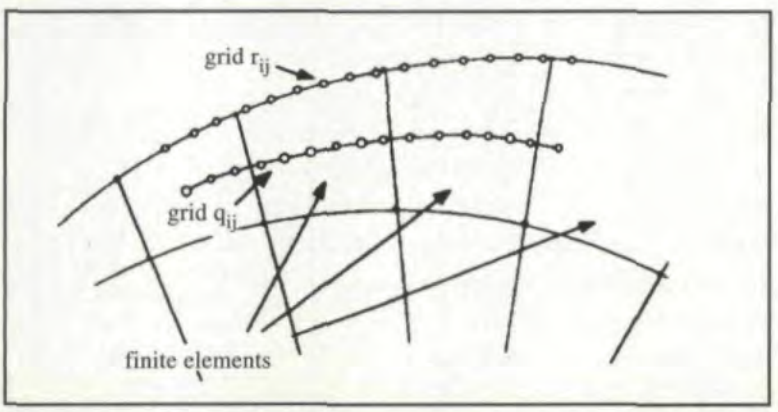

Fig. 9 — The subsurface grid q_{ij}.

Harper (Ref. 8) have used such an asymptotic matching method to determine the relative approach of two rigid cylinders pressed against an elastic cylinder in plane strain.

In order to combine the surface integral solution with the finite element solution, a reference or "matching" interface embedded in the contacting body is used. This matching surface is far enough removed from the principal point of contact so that the finite element prediction of displacements along this surface is accurate enough. At the same time, it is close enough to the principal point of contact so that the effect of the finite extent of the body does not significantly affect the relative displacement of points on this surface with respect to points in the region of contact.

Contact analysis is carried out in several steps. The first step is to lay out a grid at each contact zone. Then cross-compliance terms between the various grid points are calculated using a combination of a surface integral form of the Bousinesq and Cerruti solutions and the finite element model of the contacting bodies. Finally, load distributions and rigid body movements are calculated using an algorithm based on the Simplex method (Ref. 11).

In order to discretize the contact pressure distribution that is applied on the surfaces of two contacting gear teeth, a computational grid is set up. Fig. 6 shows such a computational grid that has been set up in the contact zone of the gears. The entire face width of one of the gears (gear 1), which is mapped onto $\{\zeta:\zeta\in[-1,+1]\}$, is divided into $2N+1$ slices. N is a user-selectable quantity. *The thickness of each slice in the* ζ *parameter* space is $\Delta\zeta = 2/(2N+1)$. For each slice, $j = -N$ *to* $+N$, a cross section of gear 1 is taken at the middle of the slice, and a point is located on this slice that approaches the surface of the mating gear (gear 2) the closest. This selection is carried out using the undeformed geometry. If the separation between the two gears at this closest point is larger than a user-selectable *separation tolerance*, then the entire gear slice is eliminated from further consideration. Otherwise, a set of grid cells identified by the grid cell location indices (i, j), $i = -M$ *to* M, and the position vector $\mathbf{r_{ij}}$ is set up centered around this closest point of slice j. The number M is user-selectable. The dimension of the grid cells in the profile direction Δs is also user-selectable.

Let $\mathbf{u}(\mathbf{p};\mathbf{q})$ denote the displacement vector at

the location $\mathbf{q}$ on a gear due to a unit normal compressive force applied at the location $\mathbf{p}$, which is on the surface of the gear. The superscripts (si) and (fe) on a term will mean that the term has been calculated using surface integral formulae and a finite element model, respectively. Subscripts 1 and 2 will denote gears number 1 and 2, respectively. When the subscript is omitted in an equation, the equation will be understood to apply to both the gears.

Let $u(\mathbf{p};\mathbf{q}) = -u(\mathbf{p};\mathbf{q})\cdot\mathbf{n}$ be the inward normal component of the displacement vector $u(\mathbf{p};\mathbf{q})$, where $\mathbf{n}$ is the outward unit normal vector at the point $\mathbf{p}$.

The displacement $u(\mathbf{r}_{ij};\mathbf{r})$ of a field point $\mathbf{r}$ due to a load at the surface grid point $\mathbf{r}_{ij}$ can be expressed as:

$$u(\mathbf{r}_{ij};\mathbf{r}) = (u(\mathbf{r}_{ij};\mathbf{r}) - u(\mathbf{r}_{ij};\mathbf{q})\ ) + u(\mathbf{r}_{ij};\mathbf{q})$$

where $\mathbf{q}$ is some location in the interior of the body sufficiently removed from the surface (Fig. 7). If the first two terms are evaluated using the surface integral formulae, and the third term is computed from the finite element model, then we obtain the displacement estimate:

$$u(\mathbf{r}_{ij};\mathbf{r})(\mathbf{q}) = (u^{(si)}(\mathbf{r}_{ij};\mathbf{r}) - u^{(si)}(\mathbf{r}_{ij};\mathbf{q}) + u^{(fe)}(\mathbf{r}_{ij};\mathbf{q})$$

The term in parentheses is the deflection of $\mathbf{r}$ with respect to the "reference point" $\mathbf{q}$. This relative component is better estimated by a local deformation field based on the Bousinesq and Cerruti half-space solutions than by the finite element model. The gross deformation of the body due to the fact that it is not a half space will not significantly affect this term. On the contrary, the remaining term $u^{(fe)}(\mathbf{r}_{ij};\mathbf{q})$ is not significantly affected by local stresses at the surface. This is because $\mathbf{q}$ is chosen to be far enough beneath the surface. This term is therefore best computed using a finite element model of the body. The value $u(\mathbf{r}_{ij};\mathbf{r})(\mathbf{q})$ thus computed will, in general, depend on the location $\mathbf{q}$ because of the different values of the surface integral and finite element displacement fields there. The location is a so-called reference or "matching" point. We would like to match the surface integral and finite element solutions not only at one point, but also at a set of points belonging to a "matching interface" (Fig. 7). We will then be interested in that value of $u(\mathbf{r}_{ij};\mathbf{r})$, which will minimize the least squares deviation:

$$\int_\Gamma [u(\mathbf{r}_{ij};\mathbf{r}) - u^{(si)}(\mathbf{r}_{ij};\mathbf{r}) - u^{(si)}(\mathbf{r}_{ij};\mathbf{q}) + u^{(fe)}(\mathbf{r}_{ij};\mathbf{q}))]^2 dr$$

where $\mathbf{q}$ varies over the reference surface Γ.

Another possibility, which lends itself better to spatial discretization is to choose a value for $u(\mathbf{r}_{ij};\mathbf{r})$ which minimizes:

$$\sum_{q\in\Gamma}[u(\mathbf{r}_{ij};\mathbf{r}) - (u^{(si)}(\mathbf{r}_{ij};\mathbf{r}) - u^{(si)}(\mathbf{r}_{ij};\mathbf{q}) + u^{(fe)}(\mathbf{r}_{ij};\mathbf{q}))]^2$$

where $\mathbf{q}$ varies over a grid of points $\mathbf{q}_{ij}$ laid out over the matching interface Γ (See Figs. 8-9). For convenience, points in this grid $\mathbf{q}_{ij}$ were chosen to lie half a finite element thickness below corresponding points in the surface grid $\mathbf{r}_{ij}$. . . . Let N be the total number of points in the grid $\mathbf{q}_{ij}$ . . . . Then the value that minimizes the least square deviation above is:

$$u(\mathbf{r}_{ij};\mathbf{r}) = (u^{(si)}(\mathbf{r}_{ij};\mathbf{r}) + \frac{1}{N}$$

$$\sum_{q\alpha\beta}[(\mathbf{r}_{ij};\mathbf{q}_{\alpha\beta}) - u^{(si)}(\mathbf{r}_{ij};\mathbf{q}_{\alpha\beta}))]^2$$

In order to obtain sufficient resolution of the contact stresses, the number of points in the grid $\mathbf{r}_{ij}$ will have to be very large, typically in the hundreds. Computation of all the terms of the type $u^{(fe)}(\mathbf{r}_{ij};\mathbf{q}_{\alpha\beta})$ would involve hundreds of back-substitutions through the decomposed finite element stiffness matrix. This would be prohibitively time-consuming because of the complexity of the three-dimensional finite element model of the body. Furthermore, the finite element model does not usually have an adequate degree of freedom at the surface to allow all the terms $u^{(fe)}(\mathbf{r}_{ij};\mathbf{q}_{\alpha\beta})$ to be independent of each other. Thus evaluating each such term by a separate back-substitution is probably also superfluous.

A better method is to obtain $u^{(fe)}(\mathbf{r}_{i(k)j(k)};\mathbf{q}_{i(l)j(l)})$ for a much smaller subset $\{\mathbf{r}_{i(k)j(k)};\ k = 1,2, \ldots ,M\}$ of the grid $\{\mathbf{r}_{ij}\}$, as shown in Fig. 10, and the corresponding subset $\{\mathbf{q}_{i(k)j(k)};\ k = 1,2, \ldots ,M\}$ of the grid $\{\mathbf{q}_{ij}\}$. If the

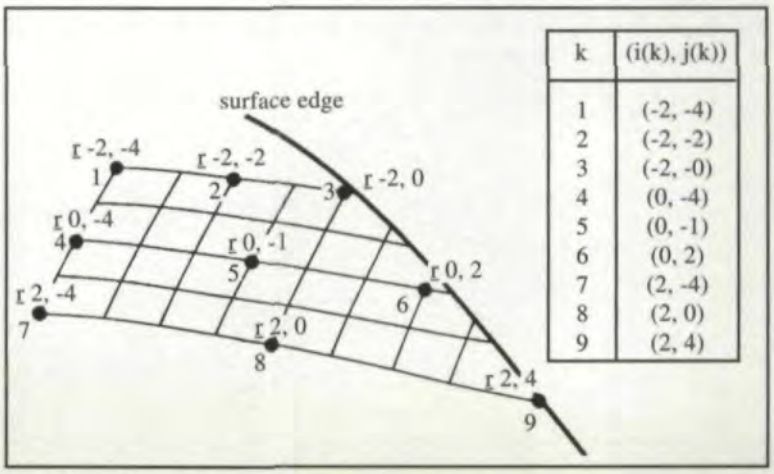

k	(i(k), j(k))
1	(-2, -4)
2	(-2, -2)
3	(-2, -0)
4	(0, -4)
5	(0, -1)
6	(0, 2)
7	(2, -4)
8	(2, 0)
9	(2, 4)

Fig. 10 — The grid subset $r_{i(k)j(k)}$.

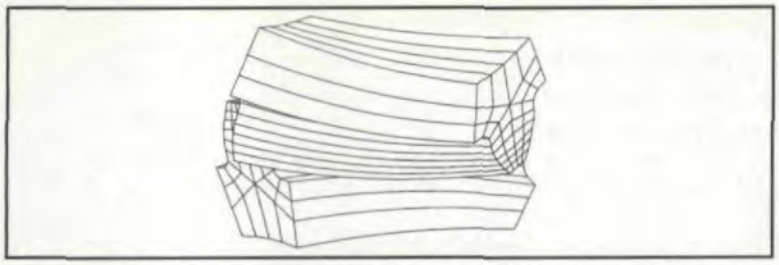

Fig. 11 — The finite element model of a pair of contacting teeth from a 90° crossed helical gear set.

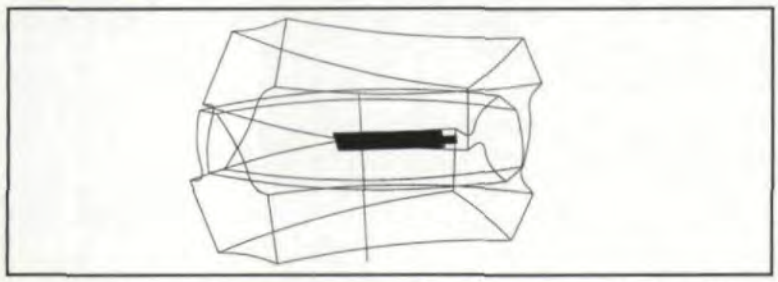

Fig. 12 — The computational grid between a pair of contacting teeth from a 90° crossed helical gear set.

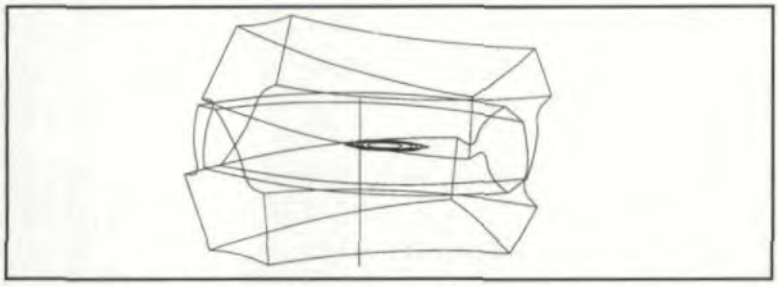

Fig. 13 — The contact pressure distribution between the contacting pair of crossed helical gear teeth.

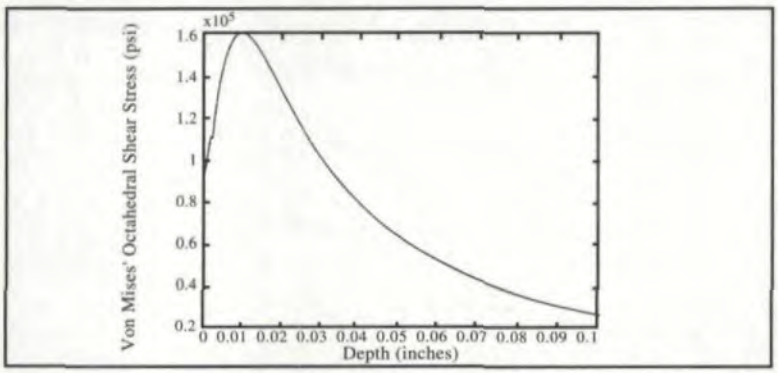

Fig. 14 — Variation of subsurface shear stress with depth under the point of maximum contact pressure.

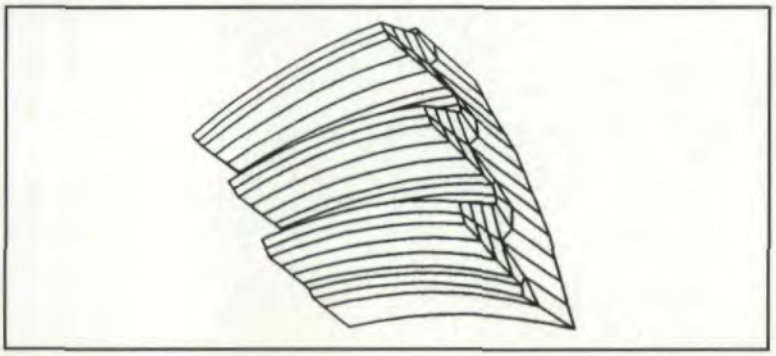

Fig. 15 — A three-tooth finite element model of the gear showing the active surfaces.

number of points M in this restricted set of grid points is small, then all the terms $u^{(fe)}(\mathbf{r}_{i(k)j(k)};\mathbf{q}_{i(l)j(l)})$ can be computed using only a small number M of back-substitutions.

In the numerical examples to follow, M was either 9 or 3. The values of $u^{(fe)}(\mathbf{r}_{ij};\mathbf{q}_{\alpha\beta}\}$ for the complete set of grid points can be obtained by using two-dimensional interpolants set up on the surface grid $\mathbf{r}_{ij}$ and the subsurface grid $\mathbf{q}_{ij}$, by the interpolation method:

$$u^{(fe)}(\mathbf{r}_{ij};\mathbf{q}_{\alpha\beta}) = \sum_{k,l=1,M} u^{(fe)}(\mathbf{r}_{i(k)j(k)};\mathbf{q}_{i(l)j(l)})N_l(\alpha,\beta)\,N_k(i,j)$$

Where the functions $N_k(i,j)$ are biquadratic functions of i and j:

$$N_k(i,j) = \sum_{\alpha,\beta=0,1,2} {}^{a}k\alpha\beta^{i^{\alpha}j^{\beta}}$$

The coefficients $a_{k\alpha\beta}$ are chosen such that

$$N_k(i(l)\ j(l) = \delta_{kl}$$

where δ_{kl} is the Kronecker delta.

The finite element formulation that was used to evaluate the terms $u^{(fe)}(\mathbf{r}_{i(k)j(k)};\mathbf{q}_{i(l)j(l)})$ has been discussed in considerable detail in earlier papers (Refs. 10, 12).

The method described above is used to calculate all the terms $u_1(\mathbf{r}_{1ij};\mathbf{r}_{1kl})$ and $u_2(\mathbf{r}_{2ij};\mathbf{r}_{2kl})$ to build a compliance matrix. The contact force distribution over the grid and rigid body motions are determined by setting up the contact equations using this compliance matrix, and solving these contact equations by any of the numerous methods available in the literature. In the numerical examples described below, a method based on the Simplex algorithm of linear programming was used. Readers are referred to Reference 11 for more details.

Numerical Examples

The following examples have been chosen to illustrate a few of the features of CAPP.

Crossed Axis Helical Gear Set. The first example shown in this article is that of a pair of identical helical gears whose axes are at right angles and whose operating helix angle is 45°. This makes an interesting example because the location and orientation of the contact zone can be easily predicted by simple calculations and by using the symmetry of the situation. Figs. 11-12 show a pair of contacting teeth of the 90° crossed

helical gear set. Fig. 11 shows the finite element meshes of the two teeth, and Fig. 12 shows a contact grid that has been set up in the contact zone. The diametral pitch of this gear set is 10. Fig. 13 shows the contact pressure distribution between the teeth as calculated by CAPP. Fig. 14 shows the variation of subsurface Von Mises' shear stress as a function of depth below the point of maximum contact pressure.

Hypoid Gear Set. The next case chosen here is that of contacting hypoid gears. The cutting machines used to manufacture these gears have many kinematic settings. The settings are chosen such that the contact zone remains in the center of the tooth surfaces as the gears roll against each other. A heuristic procedure is available to select the settings, but in practice these setting have to be selected after a tedious iterative process involving cutting and testing actual gears. Even so, it is very difficult to predict the actual contact stresses, fatigue life, kinematic errors, and other design criteria, especially when not installed in ideal conditions. The contact stresses are so sensitive to the actual surface profile that conventional 3-D contact analysis is not feasible.

A sample 90° hypoid gear set from the rear axle of a commercial vehicle was selected. The gear ratio of this set was 41:11, and the axial offset was 1.5 inches. The gear surfaces had been experimentally shown to be ideal for this particular gear ratio and axial offset. In other words, the contact zone was found to remain in the central portion of the gear teeth in the operational torque range. The object of this numerical study is to verify this by looking at the manner in which the contact pattern shifts when the gears are moved around from their ideal locations.

The model was constructed by first generating values of coordinate normal vectors for points on the surface by simulating the gear cutting machines. The finite element description of the surface was then created by fitting tenth-order truncated Chebyshev series approximations to this data. The interior portions of the finite element were created semi-automatically. Only a sector containing three teeth of each gear was modeled, with each tooth being identical. The gear (gear 1) and the pinion (gear 2, the smaller gear) were then oriented in space as per the assembly drawings, and the analysis was carried out for each individual time step. Fig. 2 shows the six-tooth gear and pinion model. Sectoral

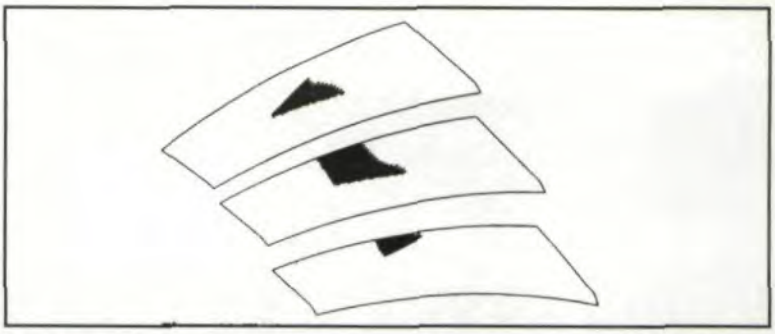

Fig. 16 — The locus of the contact zone at a gear torque of 240 in-lbs.

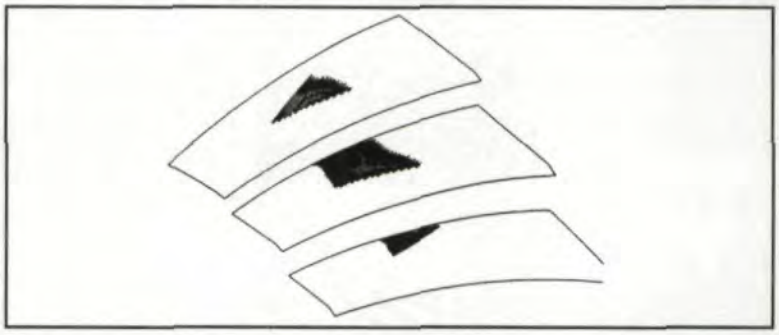

Fig. 17 — The locus of the contact zone at a gear torque of 480 in-lbs.

Fig. 18 — The locus of the contact zone at a gear torque of 960 in-lbs.

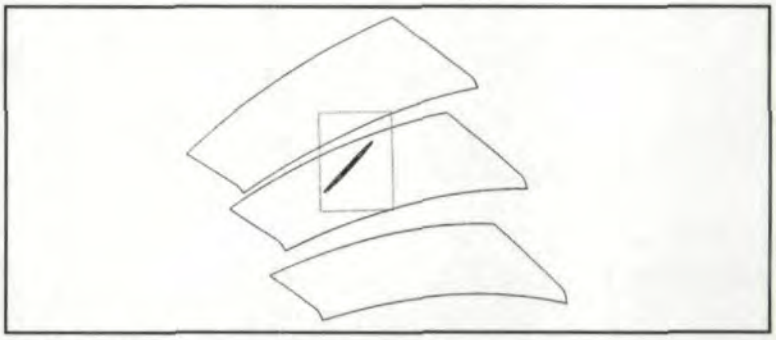

Fig. 19 — Contact pressure contours for Position 1.

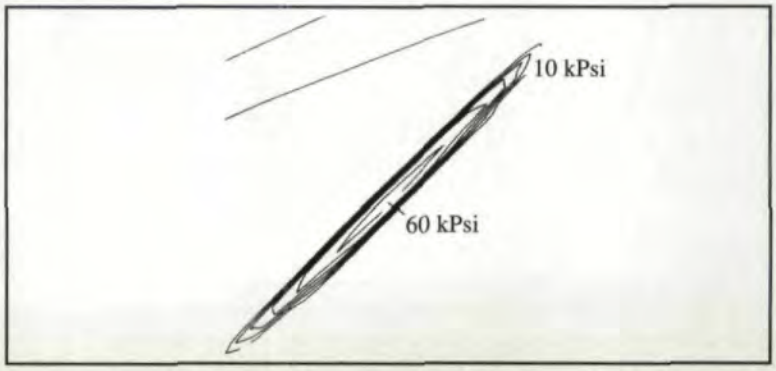

Fig. 20 — Contact pressure contours for Position 1 magnified.

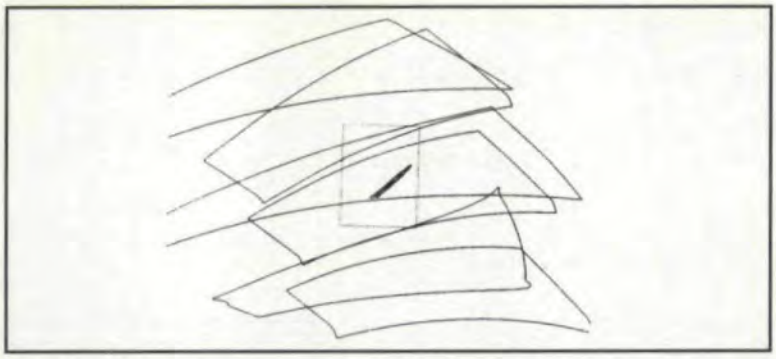

Fig. 21 — Contact pressure contours for Position 2.

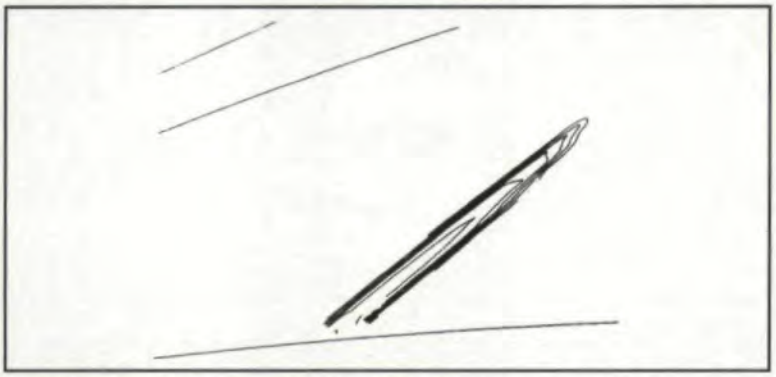

Fig. 22 — Contact pressure contours for Position 2 magnified.

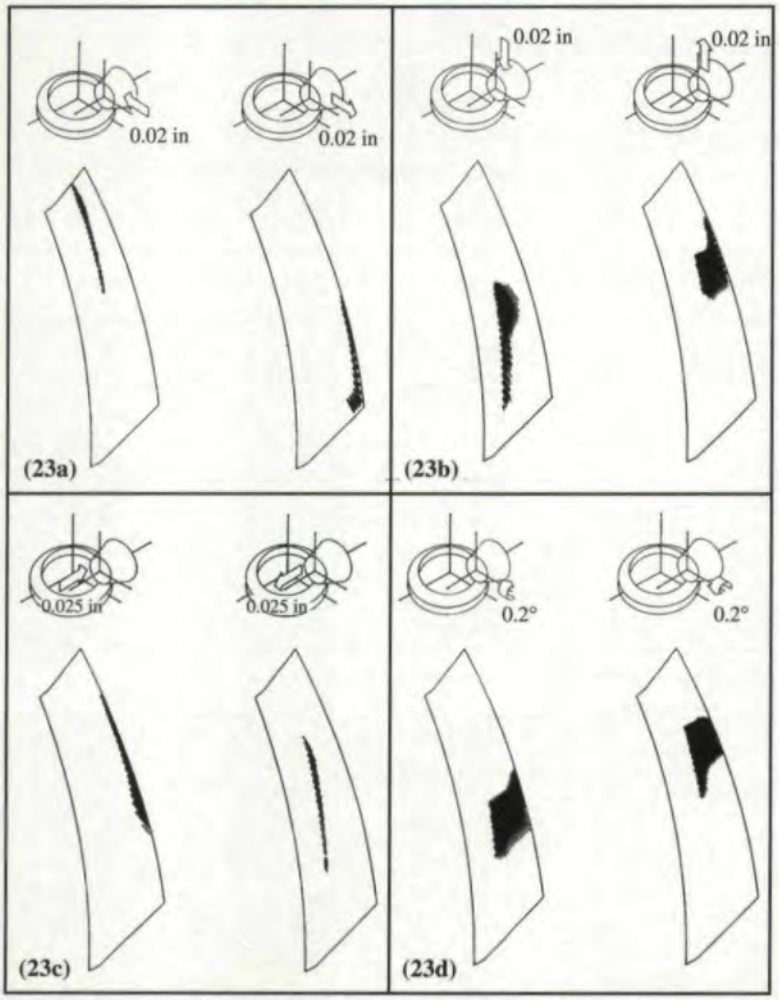

Fig. 23a — The effect of an X translation on the contact pattern.
Fig. 23b — The effect of a Y translation on the contact pattern.
Fig. 23c — The effect of a Z translation on the contact pattern.
Fig. 23d — The effect of an X rotation on the contact pattern.

symmetry is used to generate stiffness matrices from the stiffness matrix of one tooth. For this particular gear set, a three-tooth model suffices because at the most two teeth contact at a time. Fig. 15 shows the surfaces of the three-tooth gear. Figs. 16-18 show the contact pattern (which is the locus of the contact zone as the gears roll against each other), for a gear torque of 240, 480, and 960 in-lbs, respectively. Figs. 19 and 21 show views of the contact zone with contact pressure contours on the gear for two particular angular positions. Figs. 20 and 22 show magnified views of the contact zone for these two positions. They show contours of normal contact pressures on the surfaces. Computational grids of 11 x 25 cells were used on these surfaces to obtain the pressure distributions. Finally, the position of the pinion was perturbed slightly from the design location, and Figs. 23a-d show the contact patterns that were obtained. When compared to the contact pattern for the unperturbed position in Fig. 16, it shows that the best contact pattern does indeed occur at the designed position, lending credence to the notion that an analysis of the kind described in this article has the potential to be used in the design process itself.

Examples of Other Post-Processing Features. A variety of post-processing options are available for the display of the state of stress in contacting gears. Fig. 24 shows contour curves of maximum principal normal stress calculated at various sections in a pair of contacting helical gear teeth. Fig. 25 shows contour curves of maximum principal normal stress drawn along the surface of the gear tooth, and Fig. 26 shows a contour surface of maximum principal normal stress within a gear tooth. It is also possible to draw contour curves and surfaces for the minimum principal normal stress, and the Von Mises' octahedral shear stress. Fig. 27 is an example of an arrow diagram that can be used to show both the magnitude as well as direction of the principal normal stresses. Stresses are depicted by arrows pointing in the principal directions. Tensile stresses are depicted by outward pointing arrows, and compressive stresses are depicted by inward pointing arrows. The length of an arrow is proportional to the magnitude of the principal stress.

Conclusions

Using a combination of finite element and surface integral methods seems to be, in the authors' opinion, the most practical method of

modelling stiffness behavior of contacting bodies. When this method is used along with an efficient algorithm for solving contact equations, one can predict contact stress distributions and deformations in more realistic detail than otherwise possible. Results obtained from a contact analysis program (CAPP) based on this methodology have been found to compare well with calculations based on other methods. ■

References:

1. Bathe, K. and A. Chowdhury, "A Solution Method for Planar and Axisymmetric Contact Problems," *International Journal of Numerical Methods in Engineering*, 21 (1985), pp. 65-88.

2. Chowdhury, Anil and Klaus Jurgen Bathe, "A Solution Method for Static and Dynamic Analysis of Three-Dimensional Contact Problems with Frictions," *Computers and Structures*, 24 (1986), pp. 855-873.

3. de Mul, J. M., J. J. Kalker and B. Fredriksson, "The Contact Between Arbitrarily Curved Bodies of Finite Dimensions," *J. Tribology Trans. ASME*, 108 (1986), pp. 140-148.

4. Kornhauser, Murray. "A Note on Elastic Surface Deformation," *Journal of Applied Mechanics*, 18 (1951), pp. 251-252.

5. Krenzer, T. "Gear Sound Analysis-I", Sheet No. 9, Engineering Report No. 4731, (1973), Gleason Works, Rochester, NY.

6. Lai, W. T. and H. S. Cheng. "Computer Simulation of Elastic Rough Contacts," *ASLE Transactions*, 28 (1985), pp. 172-180.

7. Lubrecht, A. A., W. E. ten Napel and R. Bosma. "Multigrid, an Alternative Method of Solution for Two-Dimensional Elastohydrodynamically Lubricated Point Contact Calculations," *J. Tribology Trans. ASME*, 109 (1987), pp. 437-443.

8. Schwartz, J. and E. Harper. "On the Relative Approach of Two-Dimensional Bodies in Contact." *Int. J. Solids Structures*, 7 (1971), pp. 1613-1626.

9. Seabra, J. and D. Berthe. "Influence of Surface Waviness on the Normal Pressure Distribution in the Hertzian Contact," *J. Tribology Trans. ASME*, 109 (1987), pp. 462-470.

10. Vijayakar, S., H. Busby and D. Houser. "Finite Element Analysis of Quasi-Prismatic Bodies Using Chebyshev Polynomials." *International Journal for Numerical Methods in Engineering*. 24 (1987), pp. 1461-1477.

11. Vijayaker, S. H. Busby and D. Houser. "Linearization of Multibody Frictional Contact Problems," *Computers and Structures*, 29 (1988), pp. 569-576.

12. Vijayakar, S. H. Busby and L. Wilcox. "Finite Element Analysis of Three-Dimensional Conformal Contact With Friction." *Computers and Structures*, 33 (1989), pp. 49-62.

13. Vijayakar, S. "A Combined Surface Integral and Finite Element Solution for a Three-Dimensional Contact Problem," *International Journal for Numerical Methods in Engineering*, 31 (1991), pp. 524-546.

14. Weber, C. *The Deformations of Gears and Their Load Carrying Capacity*. Research Report 3, British Department of Scientific and Industrial Research, 1949.

15. Weber, C. "Formanderung und Profilrucknahme bei Gerad- und Schragverzahnten Radern.", *Schriftenreihe Antriebstechnik Heft II*, 1953.

Acknowledgement: *Originally presented at the AGMA Fall Technical Meeting, 1991. Reprinted with permission. The opinions, statements, and conclusions presented are those of the authors and in no way represent the position or opinion of AGMA.*

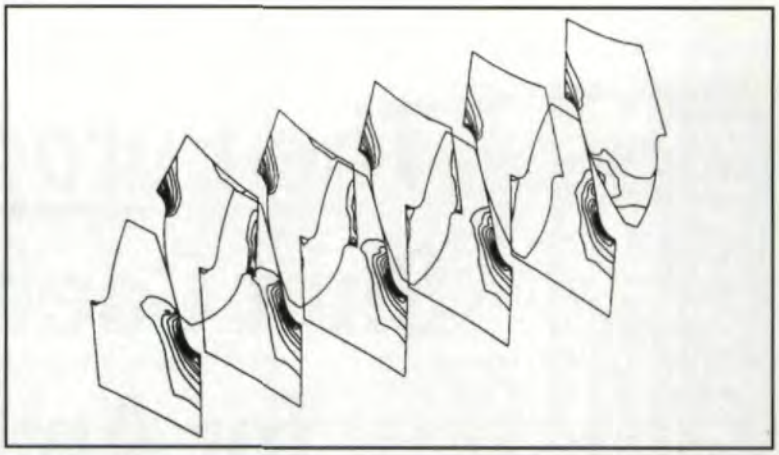

Fig. 24 — Contour curves of maximum principal normal stress drawn within sections of a contacting pair of helical gear teeth.

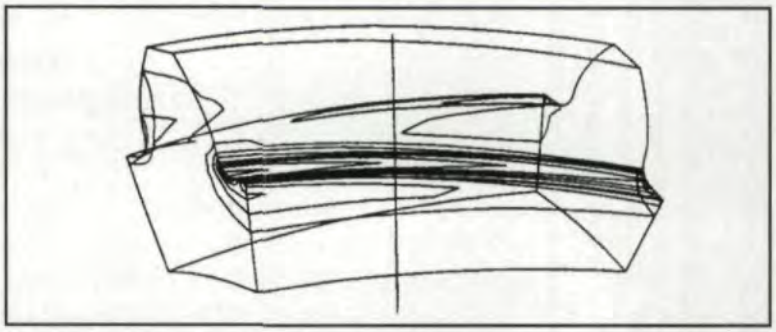

Fig. 25 — Contour curves of maximum principal stress drawn along the surface of a tooth of a crossed helical gear set.

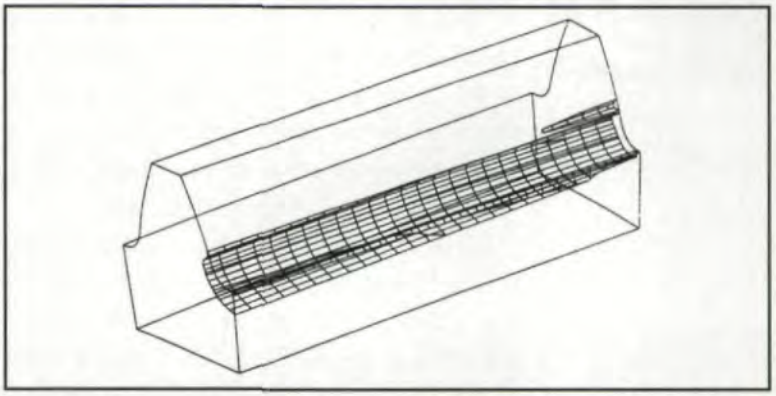

Fig. 26 — A contour surface of maximum principal normal stress within a tooth of a helical gear set.

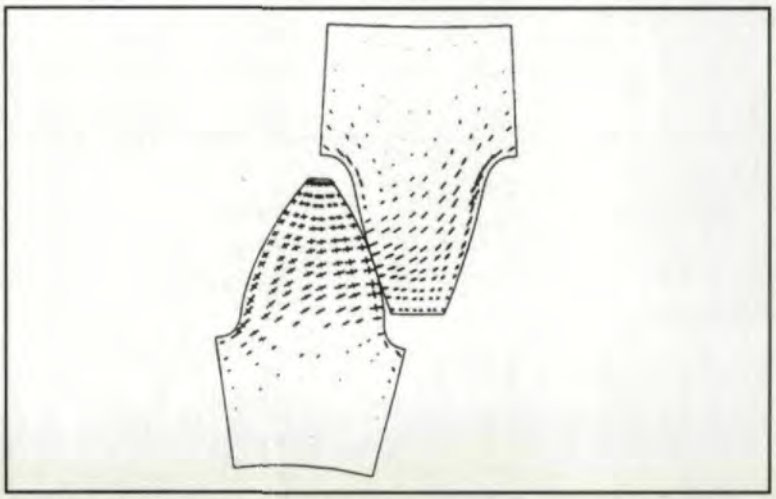

Fig. 27 — A stress arrow diagram.